ORIGINAL PAPER

In silico prediction of potential inhibitors for SARS-CoV-2 Omicron variant using molecular docking and dynamics simulation-based drug repurposing

Eslam A. R. Mohamed[1] · Islam M. Abdel-Rahman[2] · Magdi E. A. Zaki[3] · Ahmad Al-Khdhairawi[4] · Mahmoud M. Abdelhamid[5] · Ahmad M. Alqaisi[6,7] · Lyana binti Abd Rahim[8] · Bilal Abu-Hussein[9,10] · Azza A. K. El-Sheikh[11] · Sayed F. Abdelwahab[12] · Heba Ali Hassan[13]

Abstract

Background In November 2021, variant B.1.1.529 of severe acute respiratory syndrome coronavirus 2 (SARS-CoV-2) was identified by the World Health Organization (WHO) and designated Omicron. Omicron is characterized by a high number of mutations, thirty-two in total, making it more transmissible than the original virus. More than half of those mutations were found in the receptor-binding domain (RBD) that directly interacts with human angiotensin-converting enzyme 2 (ACE2). This study aimed to discover potent drugs against Omicron, which were previously repurposed for coronavirus disease 2019 (COVID-19). All repurposed anti-COVID-19 drugs were compiled from previous studies and tested against the RBD of SARS-CoV-2 Omicron.

Methods As a preliminary step, a molecular docking study was performed to investigate the potency of seventy-one compounds from four classes of inhibitors. The molecular characteristics of the best-performing five compounds were predicted by estimating the drug-likeness and drug score. Molecular dynamics simulations (MD) over 100 ns were performed to inspect the relative stability of the best compound within the Omicron receptor-binding site.

Results The current findings point out the crucial roles of Q493R, G496S, Q498R, N501Y, and Y505H in the RBD region of SARS-CoV-2 Omicron. Raltegravir, hesperidin, pyronaridine, and difloxacin achieved the highest drug scores compared with the other compounds in the four classes, with values of 81%, 57%, 18%, and 71%, respectively. The calculated results showed that raltegravir and hesperidin had high binding affinities and stabilities to Omicron with $\Delta G_{binding}$ of -75.7304 ± 0.98324 and -42.693536 ± 0.979056 kJ/mol, respectively. Further clinical studies should be performed for the two best compounds from this study.

Keywords B.1.1.529 · COVID-19 · Drug score · Molecular docking · Molecular dynamics · Omicron

Introduction

As established previously, the emergence of coronavirus disease in 2019 (COVID-19) has been attributed to severe acute respiratory syndrome coronavirus 2 (SARS-CoV-2) [1–3]. Since its discovery in December 2019, SARS-CoV-2 has been undergoing a series of mutations that have resulted in increased transmissibility and notable resistance [4, 5]. Consequently, many virus lineages were declared variants of concern (VOCs) by the World Health Organization (WHO). The reported VOCs first began in the UK as B.1.1.7 (alpha). Then, B.1.351 (beta) was reported in South Africa. The third, P.1 (Gamma) has appeared in Brazil. Recently, B.1.617.2 (Delta) and B.1.1.529 (Omicron) were recognized in India and South Africa, respectively.

SARS-CoV-2 Omicron was first discovered in late November 2021 as a multi-mutagenic virus that is rapidly spreading worldwide. Newly approved vaccines showed no effect on Omicron [6, 7]. What is also distinguishable in Omicron is that thirty amino acids were substituted in the spike protein (S-protein) as compared to the SARS-CoV-2 wild type. Fifteen amino acid substitutions out of them are located in the receptor-binding domain (RBD). The main

✉ Heba Ali Hassan
   heba.ali@pharm.sohag.edu.eg

Extended author information available on the last page of the article

crucial function of RBD is its ability to bind to the human angiotensin-converting enzyme 2 (hACE2) receptor, which exists on the surface cells of the throat and the epithelial cells of the lung [8, 9]. This binding results in a fusion between the S-protein and the cell membrane of human cells, which causes replication of the genetic materials within the cells of the host [10]. Studies associated with the in vitro protocol suggest that two mutations, namely Q498R and N501Y, are the main cause of the increased binding affinity in the RBD-hACE2 complex [11].

In the current situation, there is an urgent need for potential anti-viral agents to stop the spread of the virus. To achieve this goal, the approach of "drug repurposing" was chosen as a rapid way to inhibit Omicron activity. The key features of the repurposing approach are time saving, cost saving, and efficacy, as well as the use of FDA-approved drugs [12, 13]. The current study inspected four classes containing previously used anti-COVID-19 drugs using various in silico methods. Figure 1 shows a schematic illustration of the in silico approaches used in the filtration process and the selected classes of inhibitors.

Mefloquine [14], artemisinin [15], chloroquine, and hydroxychloroquine [16] are the main anti-malarial drugs that were previously tested as COVID-19 inhibitors [17–26]. In the class of anti-inflammatory drugs, dexamethasone [27, 28], hesperidin [29], diosmin [30], and colchicine [31] were recorded as potential COVID-19 inhibitors. In respect of anti-HIV drugs [32–47], darunavir [48], raltegravir, indinavir, and etravirine proved their efficacy [40]. Through searching in previous studies, antibiotics, specifically fluoroquinolones, were used to counter COVID-19 infection [49–57]. Levofloxacin, moxifloxacin, and ciprofloxacin were the most commonly utilized anti-COVID-19 antibiotics [58, 59].

The main objective of this study is to identify the best drug from each class to inhibit the activity of Omicron and limit its spread. As a first step, a molecular docking study was performed to determine the potential activity of all inhibitors. Based on the estimated docking scores, the molecular properties of the five highest-ranked inhibitors were evaluated. Using the drug-likeness values and drug scores, molecular dynamics simulations (MD) were performed over 100 ns, followed by binding energy calculations using a molecular mechanics-generalized Born surface area (MM/GBSA) approach implemented for the best inhibitor from each class. The results obtained in this project suggest that the identified compounds could be used to inhibit the activity of the newly emerged Omicron variant of SARS-CoV-2, which should be studied in vitro and in vivo.

Computational methodology

Protein selection and preparation

In view of the molecular docking study, the recently deposited 3D-crystal structure of the receptor-binding domain of Omicron (O-RBD) in a protein data bank (PDB) was chosen and subsequently prepared (PDB ID: 7QNW, 2.40 Å). Assigning the protonation state of 7QNW amino acids was done using the H + + server (http://biophysics. cs.vt.edu/H + +). In addition, all missed hydrogen atoms were added [60, 61]. To investigate pKa for residues, some parameters were adjusted in the H + + server such as external dielectric, internal dielectric, salinity, and pH to be equaled to 80, 10, 0.15, and 6.5, respectively.

Fig. 1 Schematic representation of the overall workflow applied in the current study
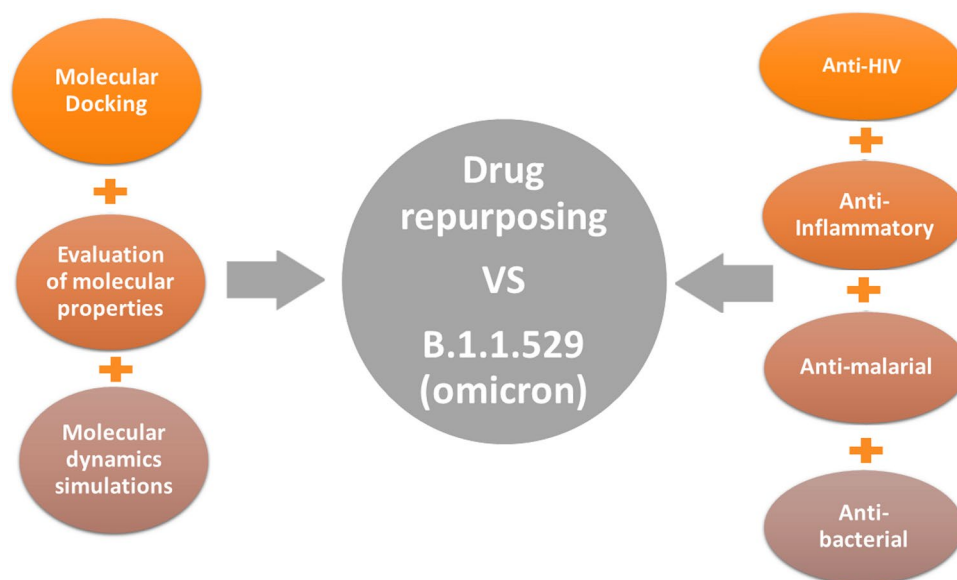
Ligand preparation

In the present study, seventy-one drugs from the four major anti-viral classes were examined to determine the likely interaction of each category against O-RBD. The structures of the tested compounds were obtained from the PubChem database (https://pubchem.ncbi.nlm.nih.gov) and stored in Spatial Data File (SDF) format. In addition, molecular minimization using the MM2 force field was performed using Chem3D Pro 12.0 software.

Molecular docking analysis

The main purpose of molecular docking analysis is to assign the binding free energy of the studied compounds and give an indication of to what extent the protein is inhibited through a defined value, which is called docking score. AutoDock Vina [62] is a computational program, which estimates the docking score of compounds in an accurate manner by evaluating nine binding modes of a ligand inside the protein active site. Based on the AutoDock protocol, the SARS-CoV-2 Omicron structure was converted into pdbqt format using MGTools 1.5.6 [63]. Except for the exhaustiveness parameter, which was set to 200, all molecular docking parameters were left at their default levels. A grid box with XYZ dimensions of $25 \times 25 \times 25$ (Å) and a spacing value of 1.00 Å was used to comprise the mutated residues of the RBD. The grid center was located at -24.35, 21.29, and -30.735 (XYZ coordinates) for SARS-CoV-2 Omicron. All nine poses were explored and only the highest one of binding energy was considered for further investigations. Different interactions of protein–ligand complexes were inspected through BIOVIA Discovery Studio [64].

In silico evaluation of molecular properties

To determine molecular properties that are should present in drug candidates, the Osiris property explorer was used. In order to evaluate how the discovered compounds are risky, properties related to irritation, mutagenicity, tumorigenicity, and reproductive effects were tested. Furthermore, additional parameters like clogP (n-octanol–water partition coefficient), MT (molecular weight), and logS (aqueous solubility) were studied. Before implementing the molecular dynamics (MD) simulations, all of that parameters were blended to generate one unique result called drug score (DS), which shows the total drug potential. Estimation of the DS can be executed by applying the following equation:

$$DS = \prod \left(\frac{1}{2} + \frac{1}{2} S_i \right) \cdot \prod t_i$$

where (S_i) is:

$$S_i = \frac{1}{1 + e^{ap_i + b}}$$

Si symbolizes the contributions calculated instantly from cLogP ($c_{\text{octanol}}/c_{\text{water}}$), molecular weight (Mwt), and drug-likeness (pi) via the second equation which represents a spline curve. Parameters *a* and *b* are (1, 5) for logS, $(1, -5)$ for cLogP, $(0.012, -6)$ for MT, and (1, 0) for drug-likeness. t_i expresses the contributions estimated from the four main types of toxicity risk (tumorigenic, mutagenic, irritant, and reproductive).

Molecular dynamics simulations

The system was prepared using the CHARMM-GUI [65–67] interface, which was supported by the CHARMM36 force field [68]. The NAMD 2.13 software [69] was used for operating all simulations. Dimensions of the periodic boundary conditions were set at 115.2 Å^3. TIP3P explicit water solvation model [70] was employed. The CHARMM General Force Field (CGenFF) [71] was used to produce the parameters for the investigated systems. Each system was then neutralized with a sufficient number of Na+/Cl- ions. Minimization, heating, equilibration, and production steps were included in the MD protocols. All MD simulations were performed using a 2 fs time step of integration. The equilibration and production were carried out in the canonical (NVT) ensemble and the isothermal–isobaric (NPT) ensemble, respectively. Using the Nosé–Hoover–Langevin piston barostat [72], with a Langevin piston decay of 0.05 ps and a period of 0.1 ps, the pressure was set at 1 atm for the 100 ns of MD production. The Langevin thermostat [73] was used to set the temperature at 298.15 K. A distance cutoff of 12.0 Å along with a pair list distance of 16 Å was applied to short-range non-bonded interactions. The Lennard–Jones interactions were evaluated with an 8.0 Å cutoff. The particle-mesh Ewald (PME) method [74, 75] was employed to treat long-range electrostatic interactions, with a grid spacing of 1.0 for all simulation cells. The SHAKE algorithm was used to restrict all covalent bonds containing hydrogen atoms. The same procedure was applied for all MD simulations to ensure uniformity.

Binding energy calculations

For the relative binding energy estimates, the molecular mechanics-generalized Born surface area (MM/GBSA) procedure executed in the MOLAICAL code was used. This can be described by using the following equations,

$$\Delta G_{binding} = \Delta G_C - \Delta G_P - \Delta G_L$$

$$\Delta G_{binding} = \Delta H - T\Delta S = \Delta E_{MM} + \Delta G_{Sol} - T\Delta S$$

where ΔG_C, ΔG_P, and ΔG_L represent the binding energy value of the complex, protein, and ligand, respectively. As well, ΔE_{MM}, ΔG_{Sol}, and $-T\Delta S$ represent the gas phase molecular mechanics change, the solvation Gibbs energy, and the conformational entropy, respectively. The term ΔE_{MM} is equal to the total of changes in electrostatic energies added to the van der Waals energies and the internal energies. The term ΔG_{Sol} is the sum of both the polar and nonpolar solvation. The normal mode of analysis was used to compute $-T\Delta S$. For the MM/GBSA computations, the solvent dielectric constant was set to 78.5 and the surface tension constant was set to 0.03012 kJ mol^{-1}Å^2.

Results and discussion

The S- protein of SARS-CoV-2 plays a pioneering role in facilitating virus entry and fusion with the cell membrane. This is attributed to its binding to the hACE2 receptor. In recent months, a multimutated virus, the SARS-CoV-2 Omicron variant, has emerged that exhibits significantly increased infectivity. These variants are located in a specific region of residues called RBD, which ranges from 319 to 541 [76].
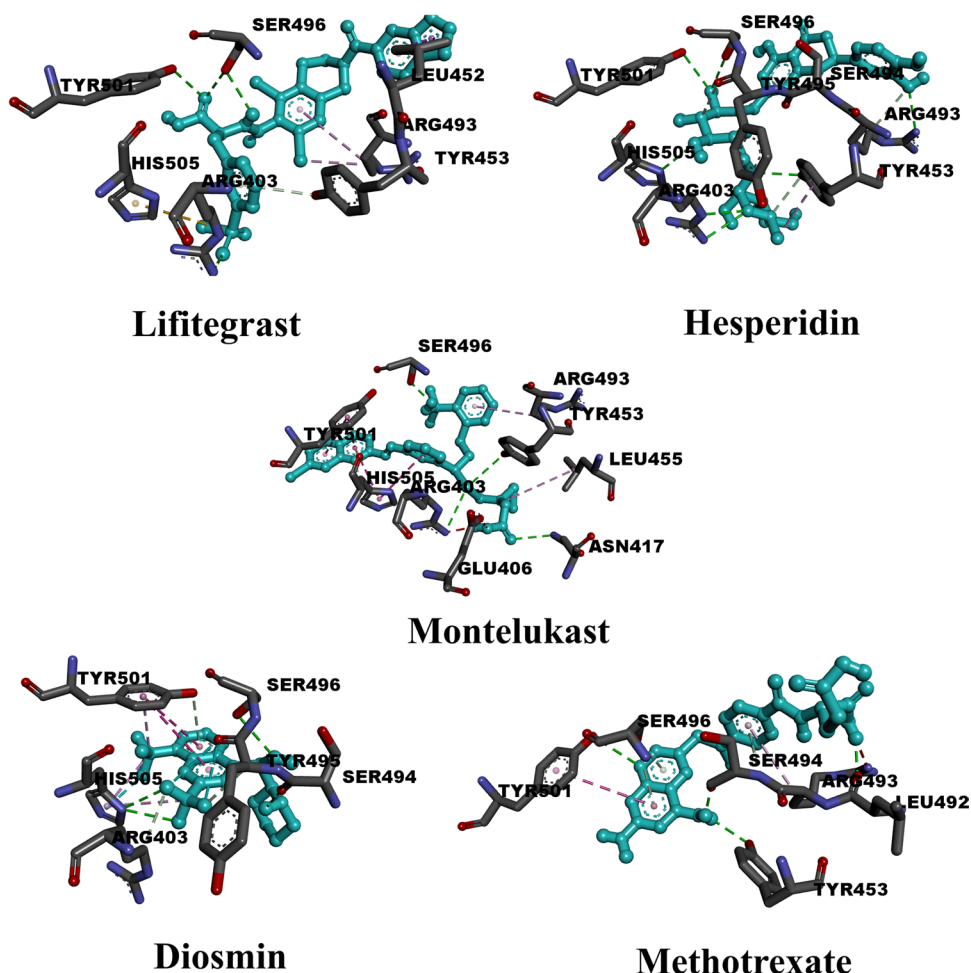
Molecular docking analysis

To explore the binding affinity of the studied compounds against the RBD of Omicron (O-RBD), an effective, accurate, and rapid computational approach called molecular docking was employed. Different types of interactions between ligand atoms and protein residues identify the extent of inhibition of the target protein. Hydrogen bonding (HB) is considered the most important of these interactions as it provides noticeable protein–ligand stability. Moreover, other types of interactions, such as pi-alkyl, pi-cation, and pi-sigma, were also observed. The molecular docking of four anti-viral classes against O-RBD, as well as binding features between each ligand and the mutated residues, was discussed and explained below.

Anti-inflammatory drugs

Fifteen anti-inflammatory drugs were inspected using the molecular docking technique. Calculated results (Table S1) revealed that four compounds achieved docking scores below -6.0 kcal/mol, whereas five compounds achieved docking scores above -7.0 kcal/mol. The highest value (-8.10 kcal/mol) was scored by lifitegrast, whereas colchicine exhibited low inhibition with a value of -5.30 kcal/mol. The average value of molecular docking scores for all inspected anti-inflammatory drugs was estimated to be equal to -6.51 kcal/mol. Table S1 demonstrates the binding features of this class of inhibitors against the Omicron variant of SARS-CoV-2. Table S2 also includes the dataset of those compounds. Figure 2 depicts the full set of interactions for the top five compounds. All drugs formed more than one conventional hydrogen bond with active site residues. In detail, dexamethasone formed two hydrogen bonds with ASN417 (2.91 Å) and HIS505 (3.47 Å). Initially, for conventional hydrogen bonds, lifitegrast formed two bonds with SER496 (2.90, 2.98 Å) and a single one with ARG403 (2.89 Å) and TYR501 (2.90 Å). As well, only one carbon-hydrogen bond with TYR453 (4.05 Å) can be noticed. Regarding the pi-alkyl type of interaction, lifitegrast formed three bonds, two of them with ARG493 (3.88, 5.27 Å) and the other with LEU452 (5.00 Å). It also formed a pi-sigma interaction with LEU452 (3.89 Å). As lifitegrast contains a sulfonyl group in its structure, a pi-sulfur interaction can be noticed here with HIS505 (5.68 Å). Unlike lifitegrast, more than four conventional hydrogen bonds were made by hesperidin with residues: ARG403 (3.07 Å), TYR453 (2.95 Å), ARG493 (2.82 Å), SER496 (3.17 Å), TYR501 (3.06 Å), and HIS505 (3.21 Å). In addition, two carbon-hydrogen bonds are formed with SER494 (3.52 Å) and TYR495 (3.41 Å). Concerning other types of interactions, only one pi-alkyl interaction was formed with TYR453 (4.53 Å). Diosmin, with a docking score of -7.4 kcal/mol, exhibited less variety of interactions as in the case of hesperidin. Diosmin formed four conventional hydrogen bonds SER494 (2.68 Å), SER496 (3.11 Å), and HIS505 (3.17, 3.18 Å). As well, it formed two carbon-hydrogen bonds (ARG403; 3.65 A & TYR495; 3.40 A) and one pi-donor hydrogen bond (TYR501, 3.53 Å). Pi-alkyl interactions (TYR501, 3.78 Å & HIS505, 3.95, 4.74 Å), pi-pi stacked interactions (TYR501, 3.53 Å), and halogen interactions (TYR495, 3.42 Å & HIS505, 3.29 Å) can, also, be observed. Montelukast shows the same number of conventional hydrogen bonds as in lifitegrast and diosmin. Interacting residues that constitute those bonds were as follows: ARG403 (3.67 Å), ASN417 (3.01 Å), TYR453 (3.59 Å), and SER496 (2.24 Å). Moreover, montelukast formed one carbon-hydrogen bond with HIS505 (3.59 Å). For the first time, unfavorable donor-donor and unfavorable acceptor-acceptor interaction occurred with ARG403 (2.13 Å) and GLU406 (2.92 Å), respectively. Further types of interactions can be detected such as pi-pi stacked interactions (TYR501, 4.12 Å & 4.96 Å, HIS505, 4.58 Å), pi-pi T-shaped interactions (HIS505, 5.15 Å), and pi-alkyl interaction (LEU455, 5.08 Å & ARG493, 5.04 Å). Figure S1 specifies the number of hydrogen bonds formed by each residue in O-RBD to show which one contributes the most. In the same way as anti-HIV drugs, SER496 and TYR501 have the main contribution in forming hydrogen bonds.

Fig. 2 3D representations of binding modes of the best five anti-inflammatory drugs based on the estimated values of docking score


Lifitegrast

Hesperidin

Montelukast

Diosmin

Methotrexate

Anti-malarial drugs

Sixteen anti-malarial agents have been tested as potential inhibitors of the Omicron variant of SARS-CoV-2. The dataset for those compounds is listed in Table S3. The binding features and molecular docking data of the sixteen protein–ligand complexes are summarized in Table S4. From the data in Table S4, all sixteen ligands formed hydrogen bonds of different lengths. The range of scores of molecular docking is from − 5.3 kcal/mol (chloroquine) to − 7.0 kcal/mol (mefloquine). The average value of the docking scores for the sixteen compounds was − 5.95 kcal/mol. Six compounds recorded values above − 6.0 kcal/mol while the other ten compounds recorded values lower than that. For the sake of getting a deep understanding of the other types of interactions in protein–ligand complexes, Fig. 3 shows the full types of interactions for the five highest compounds. What is noticed, mefloquine (− 7.0 kcal/mol) formed three basic types of hydrogen bonds. Four conventional hydrogen bonds with SER494 (2.68), SER496 (3.11 Å), and HIS505 (3.17, 3.18 Å). Two carbon-hydrogen bonds with ARG403 (3.65 Å) and TYR495 (3.40 Å). Pi-donor hydrogen bond

with TYR501 (3.53 Å). Residue TYR501 plays a vital role as it formed pi-pi stacked and pi-alkyl interaction with bond lengths equal to 5.31 and 3.78 Å, respectively. Also, HIS505 formed double interaction of pi-alkyl type with lengths equal to 3.95 and 4.47 Å. As mefloquine contains six fluorine atoms, two halogen bonds can be noticed with TYR495 (3.65 Å) and HIS505 (3.29 Å). Atovaquone, the second-highest-ranked compound regarding docking score (− 6.9 kcal/mol), formed three hydrogen bonds. One conventional hydrogen bond with TYR495 (2.30 Å) and two pi-donor hydrogen bonds with SER496 (3.47 Å) and TYR501 (3.70 Å). Remarkably, residue ARG493 formed double interactions with atovaquone that were pi-cation and pi-alky interactions. Also, pi-pi T-shaped interaction can be noticed with HIS505 (5.07 Å). Artesunate scored the highest rate of conventional hydrogen bonds with a docking score of − 6.5 kcal/mol. The interacting residues were ARG403 (4.74 Å), TYR453 (2.96, 3.06 Å), SER496 (2.73 Å), and TYR 501 (2.75 Å). Also, pi-alkyl interaction can be noticed with two residues TYR501 (4.14, 4.92, 5.06, 5.15, 6.05 Å) and HIS505 (4.50, 4.84, 5.28 Å). Although pyronaridine achieved a value of docking score equal to that

Fig. 3 3D representations of binding modes of the best five anti-malarial drugs based on the computed values of docking score

Mefloquine

Atovaquone

**Artesunate**

Pyronaridine

Artemisinin
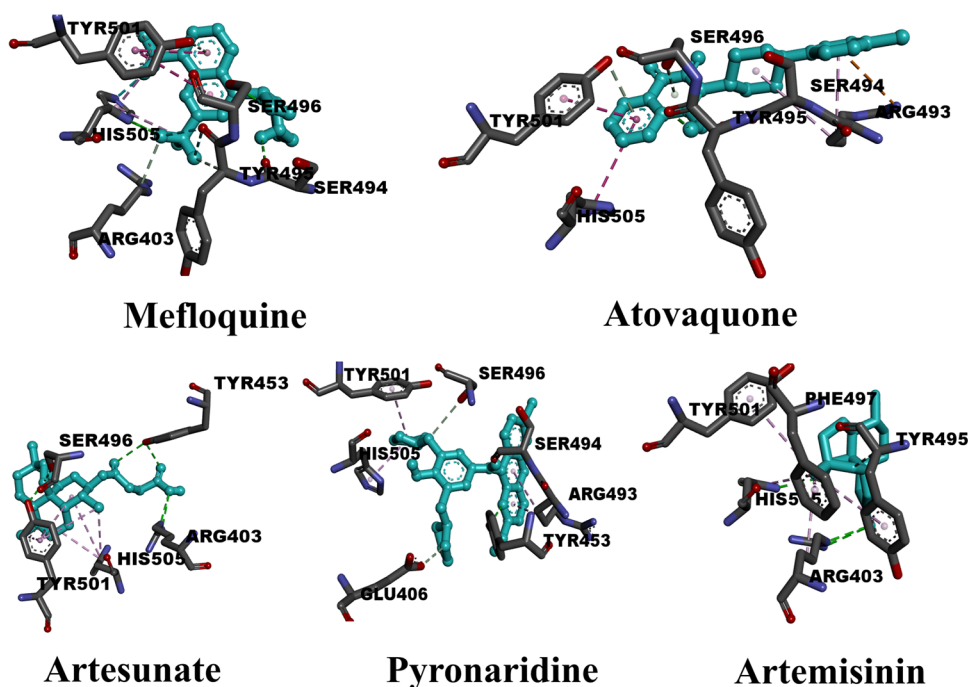
of artesunate, different types of interactions can be observed. Pyronaridine interacts with the active site of protein through conventional hydrogen bonds with SER494 (1.93 Å) and TYR453 (2.96, 3.21 Å). Similarly, pyronaridine formed two carbon-hydrogen bonds with GLU (3.75 Å) and SER496 (3.69 Å). As observed in the type of interactions that artesunate formed, pyronaridine also favors the pi-alky interaction type. The three residues that make up this type of reaction were ARG493 (4.16, 5.04 Å), TYR501 (4.48 Å), and HIS505 (4.36 Å). Artemisinin, with a value of docking score of −6.2 kcal/mol, formed three hydrogen bonds. Two of these were conventional hydrogen bonds with ARG403 (3.11 Å) and HIS505 (2.84 Å). The other hydrogen bond is a carbon-hydrogen bond with TYR495 (3.56 Å). Exceptionally, artemisinin formed five bonds of the pi-alky type with a range of bond lengths from 4.80 to 5.37 Å. The degree of interaction in the receptor-ligand complex was determined mostly by hydrogen bonding. As a result, Fig. S1 shows the number of times each class of inhibitor interacted with the O-RBD residues. In the case of inhibitors belonging to an anti-malarial class, SER496 was found to be the main residue of interaction with hydrogen bonds equal to eleven. Residue TYR501 was the second favorable residue with nine hydrogen bonds. Through four hydrogen bonds, anti-malarial drugs interacted with HIS505. Finally, residue ARG498 was identified as the residue with the fewest hydrogen bonds.

Anti-HIV drugs

Twenty anti-HIV drugs were evaluated for their potential suitability as inhibitors of the recent Omicron variant of SARS-CoV-2. The results (Table S5) showed that the docking scores of twelve of them ranged from −5.0 to −6.0 kcal/mol. Ten compounds reached values higher than −6.0 kcal/mol. Only one compound (Zalcitabine) achieved a value of less than −5.0 kcal/mol. To gain a deeper insight into the overall validity of the HIV inhibitors, the average docking score for all twenty compounds was calculated and found to be −5.96 kcal/mol. Table S5 illustrates the binding properties of this class of inhibitors against the Omicron variant of SARS-CoV-2, noting that all inhibitors except indinavir and maraviroc formed more than one hydrogen bond. Figure 4 shows the binding poses of the top five inhibitors within the active site. Interestingly, simeprevir formed multiple conventional hydrogen bonds with SER496 (2.48, 3.05 Å) and TYR501 (2.60, 2.79 Å) and a single conventional hydrogen bond with TYR449 (3.08 Å), SER494 (3.15 Å), and ARG498 (3.23 Å). It also formed a carbon-hydrogen bond with TYR453 (2.77 Å) and many pi-alkyl interactions with LEU452 (4.43, 5.15 Å), PHE490 (4.96 Å), LEU492 (4.82 Å), and HIS505 (5.04 Å). In the case of raltegravir, it formed a large number of conventional hydrogen bonds with TYR449 (2.93 Å), TYR453 (3.11 Å), ARG493 (3.61 Å), SER494 (3.02, 3.25 Å), TYR495 (2.91 Å), SER496 (2.15, 3.98 Å), ARG498 (3.10 Å), and TYR501(2.87 Å). Similar to simeprevir, raltegravir also formed a carbon-hydrogen bond with ARG403 (3.26 Å). In contrast to simeprevir, raltegravir formed only a pi-alky interaction with ARG403 (5.14 Å). As for indinavir, the TYR501 residue formed several types of interactions, such as a conventional hydrogen bond (2.90 Å), pi-pi stacked
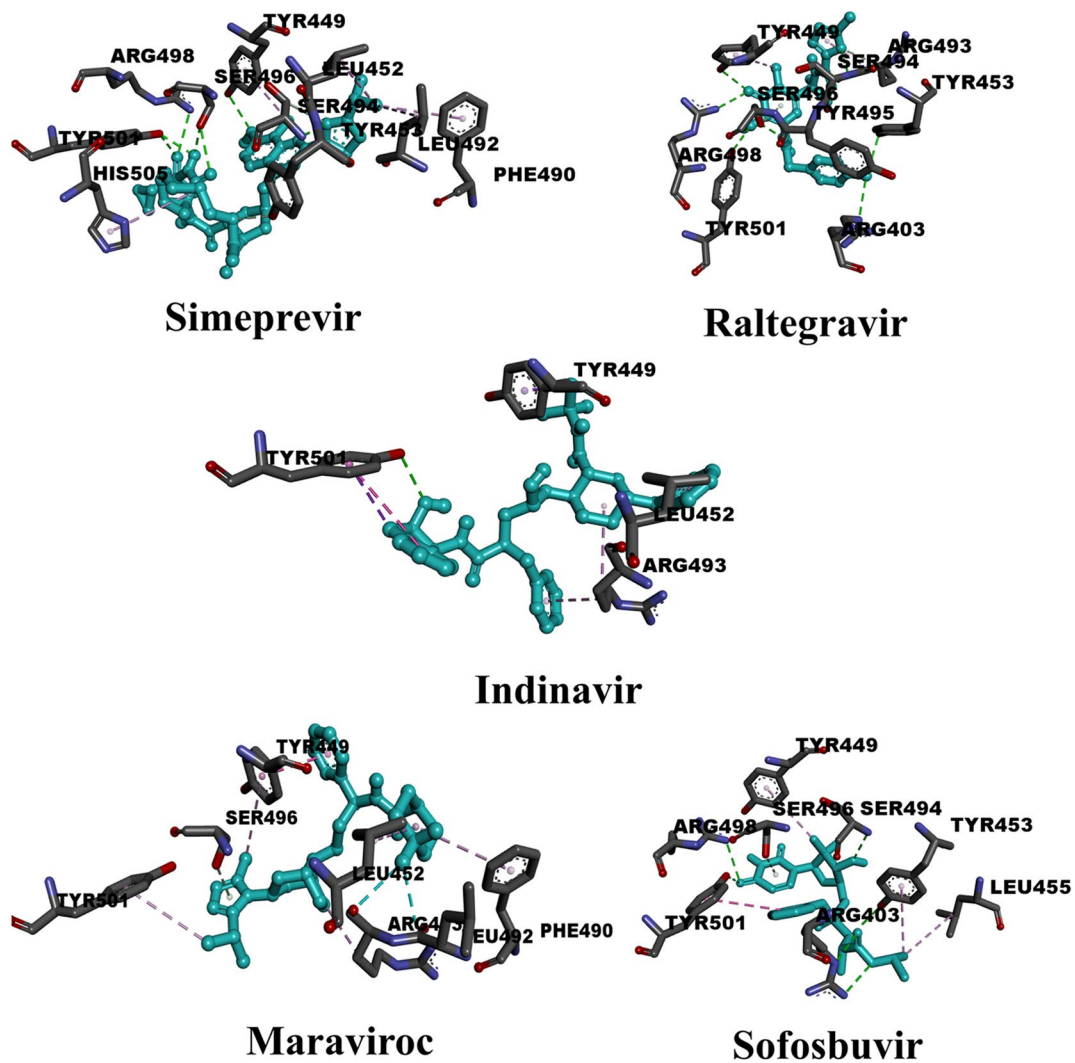
Fig. 4 3D representations of binding modes of the best five anti-HIV drugs according to the estimated values of the docking score

interaction (5.52 Å), and a pi-sigma interaction (3.79 Å). In addition, indinavir formed one pi-sigma interaction with TYR449 (3.68 Å) and two pi-alkyl interactions with LEU452 (5.06 Å) and ARG493 (4.27, 5.18 Å). Similar to indinavir, maraviroc formed a hydrogen bond, but of the carbon-hydrogen bond type with SER496 (3.07 Å). Since maraviroc contains two fluorine atoms in its structure, a halogen interaction can be observed with LEU492 (3.43 Å) and ARG493 (3.37 Å). The TYR449 residue shows a double interaction with maraviroc through pi-pi stacked interaction (3.92 Å) and a pi-alkyl interaction (5.48 Å). Additional pi-alkyl interactions were detected by maraviroc with the following residues: LEU452 (5.27 Å), PHE490 (5.16 Å), ARG493 (5.48 Å), and TYR501 (5.23 Å). Similar to simeprevir and raltegravir, sofosbuvir shows more than one conventional hydrogen bond and

only one carbon-hydrogen bond in its interaction with active site residues. Conventional hydrogen bonds can be detected with the following residues: ARG403 (3.07, 3.20 Å), SER453 (3.03 Å), SER494 (2.90 Å), ARG498 (3.16 Å), and TYR501(2.92 Å). The only carbon-hydrogen bond was with SER496 (3.80 Å). In addition, sofosbuvir formed two other types of interactions: pi-pi stacked interactions with TYR501 (5.44 Å) and pi-alkyl interactions with TYR449 (4.84 Å), TYR453 (4.87 Å), and LEU455 (4.94 Å). Finally, in Fig. S1, we analyzed the most abundant residue in O-RBD with which anti-HIV drugs preferentially interact. Strikingly, HIV inhibitors formed hydrogen bonds fifteen times with SER496, twelve times with TYR501, eleven times with SER494, eight times with ARG498, five times with HIS505, and three times with ARG493. It is clearly apparent that SER496 has the

Fig. 5 3D representations of binding modes of the best five anti-bacterial drugs according to the estimated values of docking score

Sarafloxacin

Orbifloxacin

Difloxacin

Trovafloxacin

Delafloxacin
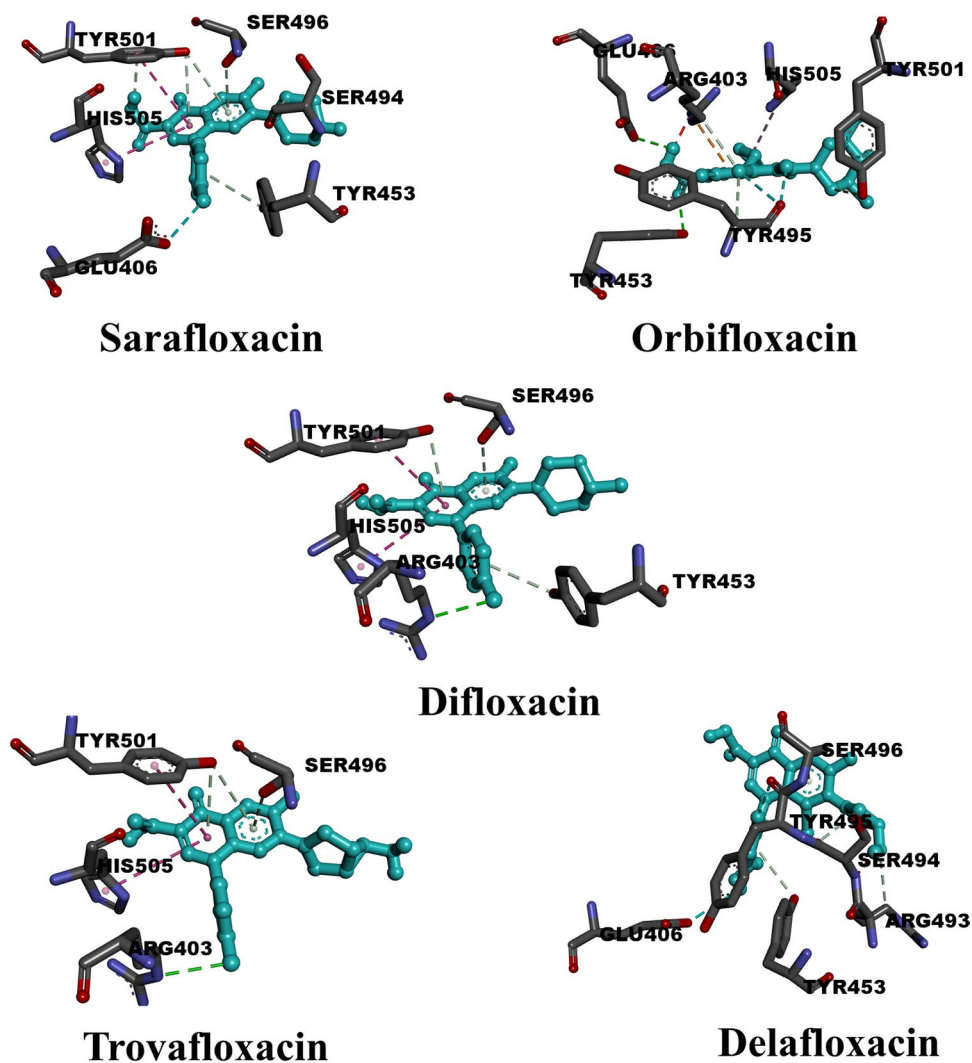
main role rather than other S-RBD residues. The dataset of those compounds is available in Table S6.

Anti-bacterial drugs

In the current study, anti-bacterial agents, particularly fluoroquinolones, were tested to determine their suitability for inhibiting Omicron. The data from the molecular docking study and the binding properties for the twenty compounds tested can be seen in Table S7, respectively. Only two compounds, namely sarafloxacin and difloxacin, achieved docking values greater than − 7.0 kcal/mol. Figure 5 shows the binding pose of the top five drugs. As expected, moderate interactions are observed in contrast to the anti-HIV, anti-inflammatory, and anti-malarial drugs. Sarafloxacin, for example, which has the highest molecular docking score did not record conventional hydrogen bonding with O-RBD residues. Delafloxacin, which ranks fourth in molecular docking score, also does not exhibit conventional hydrogen bonding.

In addition, difloxacin and trovafloxacin exhibit only conventional hydrogen bonding with the same residue ARG403. Orbifloxacin is the only fluoroquinolone that forms two conventional hydrogen bonds with GLU406 (2.91 Å) and TYR453 (2.87 Å). Although there were few conventional hydrogen bonds in this class of inhibitors, they instead formed carbon-hydrogen bonds and pi-donor hydrogen bonds. Since all drugs have the fluoroquinolone skeleton, the halogen (fluorine) interactions were the predominant binding features for most of them. Specifically, sarafloxacin formed only one carbon-hydrogen bond with SER494 (3.54 Å). It also formed five pi-donor hydrogen bonds with TYR453 (4.16 Å), SER496 (3.36 Å), and TYR501 (2.69, 4.18, 4.20 Å). Additional types of interactions were observed, such as the pi-pi T-shaped interaction (HIS505, 5.21 Å) and the halogen (fluorine) interaction (GLU406, 3.63 Å). Table S8 comprises the dataset for those compounds.

Similar to sarafloxacin, difloxacin formed a pi-pi T-shaped interaction (HIS505, 5.54 Å) and additionally three

pi-donor hydrogen bonds with TYR453 (4.18 Å), SER496 (3.55 Å), and TYR501 (3.99 Å). With a docking score of −6.80 kcal/mol, trovafloxacin also formed three pi-donor hydrogen bonds with SER496 (3.26 Å) and TYR501 (3.81, 4.06 Å). As with sarafloxacin and difloxacin, residue HIS505 also forms a pi-pi T-shaped interaction with a bond distance of 5.33 Å. No halogen (fluorine) interaction is observed in the interaction of trovafloxacin with O-RBD residues. As in the case of sarafloxacin, delafloxacin also shows pi-donor hydrogen bond interactions (TYR453, 3.95 Å & SER496, 3.48 Å) and carbon-hydrogen bond interactions (ARG493, 3.55 Å & SER494, 3.12 Å). Halogen (fluorine) interactions were registered for residues GLU406 (3.62 Å), SER494 (3.67 Å), and TYR495 (2.80 Å). In contrast to the four aforementioned inhibitors, orbifloxacin exhibited two conventional hydrogen bonds GLU406 (2.91 Å) and TYR453 (2.87 Å). The three remaining hydrogen bonds belonged to the carbon-hydrogen bond type formed with ARG403 (3.50 Å), TYR495 (3.62 Å), and TYR501 (3.52 Å). Other types of interactions can be detected for each residue. For example, a pi-cation interaction (ARG403, 4.12 Å), a pi-alkyl interaction (HIS505, 5.39 Å), and a halogen interaction (TYR495, 2.74 Å). The contribution of each residue in the O-RBD is shown in Fig. S1. Only three residues were found to form hydrogen bonds with fluoroquinolones. As with the previous classes, SER496 and TYR501 had the most contributions, each with an equal number of hydrogen bonds. Only one hydrogen bond was formed by ARG493.

In silico evaluation of molecular properties

OSIRIS Property Explorer was used to calculate drug-related characteristics such as toxicity risks, drug-likeness score, cLogP, logS, and MW. All of these parameters provide an indication of an important property of the drug under study. For example, the cLogP parameter gives an indication of lipophilicity. Similarly, the logS parameter gives an indication of hydrophilicity. As highlighted in the methodology section, Osiris has an important feature in that it can combine all these parameters into a single value called the drug score. This type of analysis was performed for the five compounds with the highest docking scores from each of the four classes. MD simulations were only performed for compounds that had a positive drug-likeness score and the highest drug score compared to their analogs from the same class.

Anti-HIV drugs

All anti-HIV drugs showed positive values of the drug-likeness score except maraviroc and sofosbuvir (Fig. 6). Consequently, maraviroc and sofosbuvir were excluded. Regarding values of drug score, raltegravir obtained the highest value,
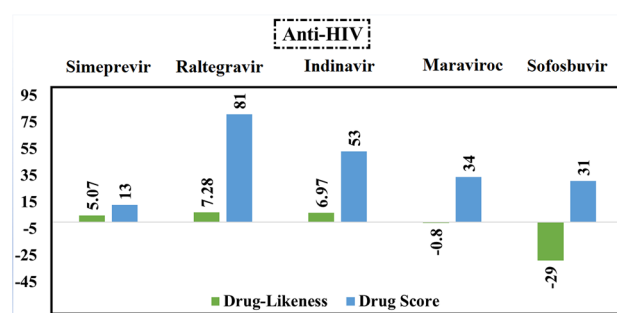
Fig. 6 Calculated values of drug-likeness and drug score of the best five anti-HIV compounds based on the data of molecular docking study

which is equal to 81%. So, raltegravir was considered for further MD simulations.

Anti-inflammatory drugs

Excluding lifitegrast and methotrexate, all anti-inflammatory drugs exhibited positive drug-likeness scores (Fig. 7). As can be observed from the data of anti-inflammatory drugs in Fig. 7, lifitegrast and montelukast achieved the same value of drug score (14%). In addition, the same drug score value (57%) was estimated for hesperidin and diosmin. According to the calculated data in the molecular docking study, hesperidin has an advantage over diosmin with a docking score of −7.8 kcal/mol. As a consequence, hesperidin was selected for the MD simulation study.
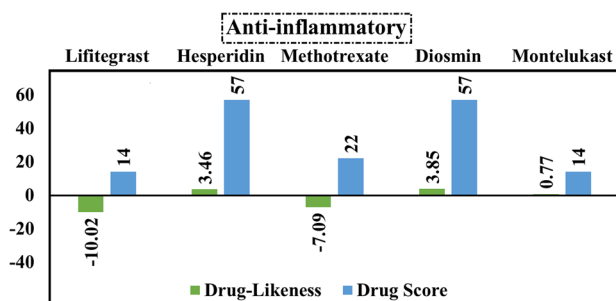
Anti-malarial drugs

What is important about the data on anti-malarial drugs (Fig. 8) is that all inhibitors achieved negative drug-likeness scores except pyronaridine. Although mefloquine has a value of drug score equal to 20%, pyronaridine (DS = 18%) was chosen for the MD simulation study as it has a positive value of drug-likeness which is equal to 1.41.

Anti-bacterial agents

It is worth mentioning that all inhibitors belonging to the anti-bacterial class exhibit positive values for drug-likeness (Fig. 9). Difloxacin obtained the highest value of both drug-likeness (5.25) and drug score (71%). Accordingly, it was considered in performing the MD simulation study.

Molecular dynamics (MD) simulations

The purpose of using MD simulations is attributed to its main role in studying conformational stability and obtaining reliable results about the behavior of the studied
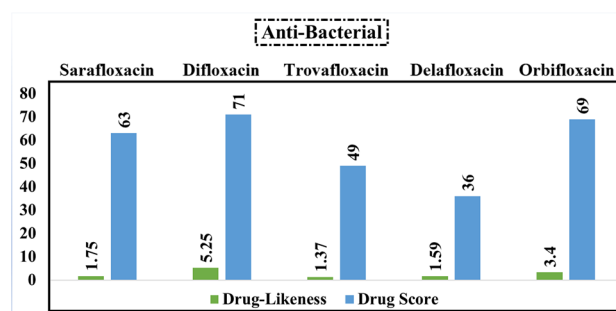
Fig. 7 Calculated values of drug-likeness and drug score of the best five anti-inflammatory compounds based on the data of molecular docking study
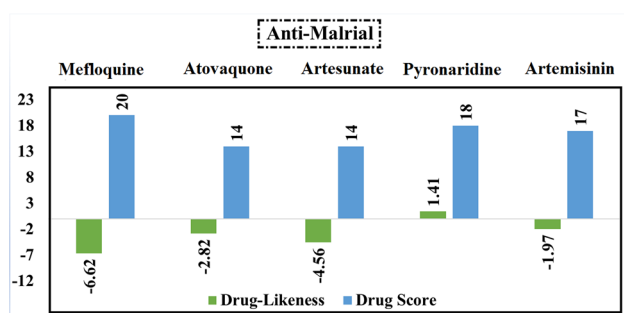
Fig. 8 Calculated values of drug-likeness and drug score of the best five anti-malarial compounds based on the data of molecular docking study

Fig. 9 Calculated values of drug-likeness and drug score of the best five anti-bacterial compounds based on the data of molecular docking study

compounds in the active site of the protein. In accordance with the results of the molecular docking study and the review of molecular properties, the best compound from each class was selected. MM/GBSA binding energy calculations studied four complexes over 100 ns MD simulations to estimate the binding behavior of the ligand to the receptor. The calculated MM/GBSA binding energies of the four protein–ligand complexes over 100 ns are shown in Table 1.

What is noticed from the data shown in Table 1 is that difloxacin, which has a docking score and drug score of -7.0 kcal/mol and 71.0%, respectively, obtained the lowest value of $\Delta G_{\text{binding}}$ of $-33.9795192 \pm 0.8330344$ kJ/mol which reflects its weak inhibition of SARS-CoV-2 Omicron. Taking into consideration the best drug from the anti-HIV class, the computed MM/GBSA binding energies revealed that raltegravir scored adequate inhibition of SARS-CoV-2 Omicron with $\Delta G_{\text{binding}}$ of -75.7304 ± 0.98324 kJ/mol. Strikingly, pyronaridine, an anti-malarial drug, scored $\Delta G_{\text{binding}}$ of $-75.8136616 \pm 0.8234112$, which is very close to the value of raltegravir. The best anti-inflammatory drug, hesperidin, showed relatively high binding affinity towards SARS-CoV-2 Omicron with a $\Delta G_{\text{binding}}$ of -42.693536 ± 0.979056 kJ/mol.

For quantitative assessment of the overall stability of raltegravir, hesperidin, pyronaridine, and difloxacin complexed with SARS-CoV-2 Omicron over 100 ns MD simulations, analyses of root-mean-square deviation (RMSD), root-mean-square fluctuation (RMSF), radius of gyration (Rg), and solvent-accessible surface area (SASA) were performed.
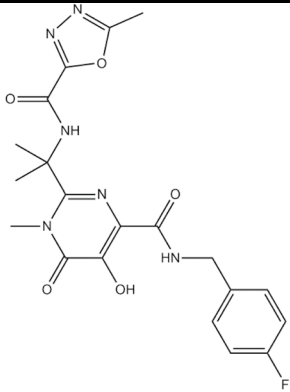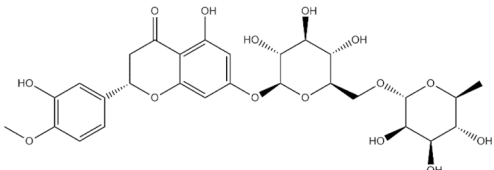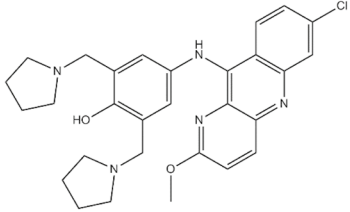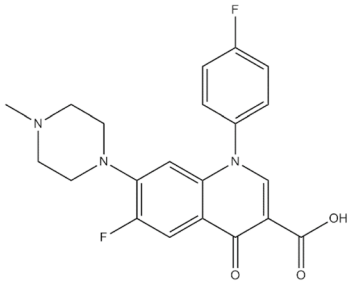
The RMSD for the four complexes under investigation was calculated to assess conformational change and the systems' stability during the 100 ns MD simulation periods [77]. Higher values of RMSD demonstrate relative instability, whereas lower RMSD values are more favorable. The RMSD plot for the four simulation systems can be witnessed in Fig. 10.

As depicted in Fig. 10, pyronaridine exhibited higher RMSD values as compared to others, which indicates its moderate stability inside the SARS-CoV-2 Omicron active site. Besides, hesperidin, with a $\Delta G_{\text{binding}}$ equal to -42.693536 ± 0.979056 kJ/mol, showed values of RMSD less than 0.21 nm. With respect to raltegravir, values of RMSD over the 100 ns MD simulations were less than 0.28 nm, which is compatible with the estimated value of binding energy (-75.7304 ± 0.98324 kJ/mol). Difloxacin, the lowest compound out of the four in terms of binding energy ($-33.9795192 \pm 0.8330344$ kJ/mol), exhibited relative instability from 70 to 100 ns. The average RMSD value of the apoprotein structure was 0.13 nm.

RMSF was employed with the aim of identifying the flexibility and fluctuation of each SARS-CoV-2 Omicron residue, in addition to how much the movement of each residue over the whole simulation period. The flexibility of each residue was investigated in an attempt to better comprehend how ligand binding influences protein flexibility during the MD simulation course. Lower values of RMSF imply better receptor compactness, stiffness, and stability. The RMSF values for the four studied complexes are figured out in Fig. 11.

What is noticed from the data in Fig. 11 is results of RMSF were nearly compatible with RMSD data. Difloxacin

Table 1 Calculated MM/GBSA binding energies (in kJ/mol) over 100 ns for the best compound in each investigated class.

Compound	PubChem ID	Structure	MM/GBSA $\Delta G_{binding}$
Raltegravir	54671008		−75.7304 ± 0.98324
Hesperidin	10621		−42.693536 ± 0.979056
Pyronaridine	107771		−75.8136616 ± 0.8234112
Difloxacin	56206		−33.9795192 ± 0.8330344
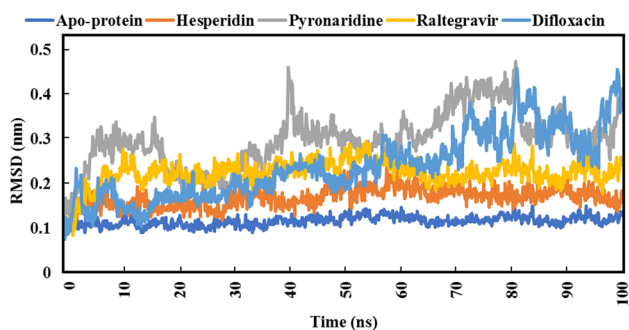
Fig. 10 Root-mean-square deviation (RMSD) SARS-CoV-2 Omicron backbone atoms from the initial structure complexed with the highest-ranked compounds over 100 ns MD simulations

and pyronaridine displayed relatively high values of RMSF, which indicate the high amino acid residues' fluctuation when complexed with those inhibitors. It is worth mentioning that raltegravir, as well as hesperidin, showed similar values of RMSF, i.e., a similar effect on fluctuations of amino acid residues. The average RMSF value of the apo-protein structure was 0.065 nm.

The Rg analysis was accomplished over 100 ns MD simulations to interpret the compactness of the protein structure inside the system [78]. Low Rg values indicate conformational stability and the degree to which the protein structure is tightly packed. Rg data is illustrated in Fig. 12.

From the beginning of 70 ns to the end of the MD simulation, raltegravir showed very close values to hesperidin.
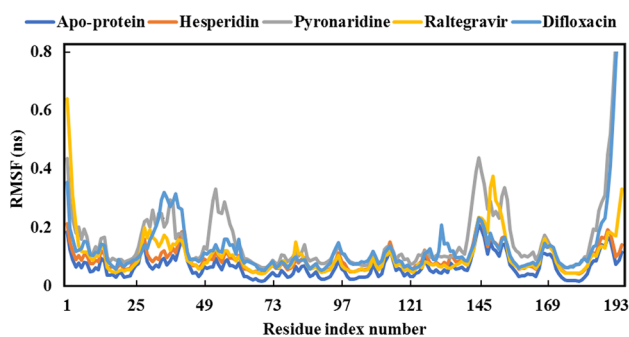
Fig. 11 Root-mean-square fluctuation (RMSF) of the apoprotein structure and five selected complexes
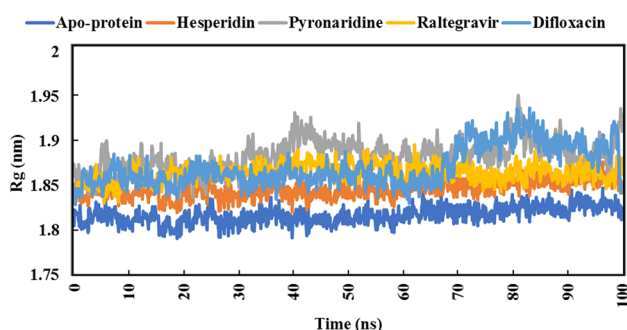
Fig. 12 Radius of gyration (Rg) plot of apoprotein structure and five identified complexes through 100 ns MD simulations

Moreover, also from 70 to 100 ns, pyronaridine and difloxacin showed remarkable overlap in Rg values. The average Rg value of the apoprotein structure was 1.81 nm.

SASA is employed to specify the surface area of the receptor that is available to a solvent [79, 80]. Figure 13 represents the data of SASA of the four compounds.

Estimated results demonstrated that hesperidin exhibited the lowest values of SASA as compared to others. On the other side, difloxacin showed an extensive increase in SASA values from 70 ns to the end of the MD simulation period. Both raltegravir and pyronaridine showed overlapping SASA values over the whole MD simulation period. The average SASA value of the apoprotein structure was 1097.15 nm^2.

Limitations of this study

The limitations of this study are as follows:

1. The 100 ns scale molecular dynamics simulation may be short to evaluate the stability of identified compounds inside the cavity, but unfortunately, we do not have enough devices to extend the simulation time up to 1,000,000 ns.
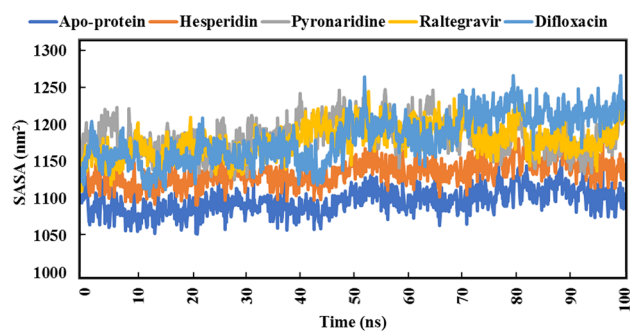
Fig. 13 Solvent-accessible surface area (SASA) of apoprotein structure and the best five compounds for 100 ns MD simulations

2. As the study was established based on drug repurposing methodology, there are previous experimental assays available on the FDA database for most of the investigated drugs. It is worth mentioning that the present study relied on estimating the physicochemical and toxicological molecular properties.
3. Other classes of inhibitors should be investigated as anti-Omicron drugs. It is worth mentioning that the current study addresses the potential activity of four classes of inhibitors, anti-HIV, anti-malarial, anti-inflammatory, and anti-bacterial, which were mentioned in the previous studies as anti-COVID-19 drugs.

Summary and conclusions

The emergence of SARS-CoV-2 Omicron led to increased viral spread and transmissibility of the virus. Amino acid variations, particularly in the RBD, are a prominent feature of Omicron. A total of seventy-one compounds from four different classes were evaluated in detail. In this study, molecular docking, prediction of drug-relevant properties using Osiris property explorer, and MD simulations were used to select the best compound in each class. According to the results, raltegravir is the best HIV inhibitor with a drug score and $\Delta G_{\text{binding}}$ of 81% and -75.7304 ± 0.98324 kJ/mol, respectively. Hesperidin (anti-inflammatory) also showed a high inhibition rate towards Omicron with a drug score and $\Delta G_{\text{binding}}$ of 57% and -42.693536 ± 0.979056 kJ/mol, respectively. On the other hand, moderate inhibition of pyronaridine (an anti-malarial) and difloxacin (anti-bacterial) was observed. The current results suggest that raltegravir and hesperidin may have potential activity against the SARS-CoV-2 Omicron variant and should be considered for further in vivo and in vitro studies.

Data availability The datasets supporting this article have been uploaded as part of the electronic supplementary material.

Declarations

Ethics approval This manuscript does not include any experiments on humans or animals.

Consent to participate The corresponding author consents on behalf of all authors.

Consent for publication The corresponding author consents on behalf of all authors.

Competing interests The authors declare no competing interests.

References

1. Lu R et al (2020) Genomic characterisation and epidemiology of 2019 novel coronavirus: implications for virus origins and receptor binding. Lancet 395(10224):565–574. https://doi.org/10.1016/S0140-6736(20)30251-8

2. Wu F et al (2020) A new coronavirus associated with human respiratory disease in China. Nature 579(7798):265–269. https://doi.org/10.1038/s41586-020-2008-3

3. Pascarella G et al (2020) COVID-19 diagnosis and management: a comprehensive review. J Intern Med 288(2):192–206. https://doi.org/10.1111/joim.13091

4. Li Q et al (2020) The impact of mutations in SARS-CoV-2 spike on viral infectivity and antigenicity. Cell 182(5):1284-1294.e9. https://doi.org/10.1016/j.cell.2020.07.012

5. Harvey WT et al (2021) SARS-CoV-2 variants, spike mutations and immune escape. Nat Rev Microbiol 19(7):409–424. https://doi.org/10.1038/s41579-021-00573-0

6. Doria-Rose NA et al (2021) "Booster of mRNA-1273 strengthens SARS-CoV-2 Omicron neutralization," medRxiv, p. 2021.12.15.21267805. https://doi.org/10.1101/2021.12.15.21267805

7. Mahase C (2021) COVID-19: do vaccines work against omicron{\textemdash}and other questions answered. BMJ 375. https://doi.org/10.1136/bmj.n3062

8. Letko M, Marzi A, Munster V (2020) Functional assessment of cell entry and receptor usage for SARS-CoV-2 and other lineage B betacoronaviruses. Nat Microbiol 5(4):562–569. https://doi.org/10.1038/s41564-020-0688-y

9. Ramanathan M, Ferguson ID, Miao W, Khavari PA (2021) "SARS-CoV-2 B.1.1.7 and B.1.3.5.1 spike variants bind human ACE2 with increased affinity. Lancet Infect Dis 21(8):1070. https://doi.org/10.1016/S1473-3099(21)00262-0

10. Ke Z et al (2020) Structures and distributions of SARS-CoV-2 spike proteins on intact virions. Nature 588(7838):498–502. https://doi.org/10.1038/s41586-020-2665-2

11. Quarleri J, Galvan V, Delpino MV (2022) Omicron variant of the SARS-CoV-2: a quest to define the consequences of its high mutational load. GeroScience 44(1):53–56. https://doi.org/10.1007/s11357-021-00500-4

12. Cheng F, Hong H, Yang S, Wei Y (2017) Individualized network-based drug repositioning infrastructure for precision oncology in the panomics era. Brief Bioinform 18(4):682–697. https://doi.org/10.1093/bib/bbw051

13. Zhou Y, Hou Y, Shen J, Huang Y, Martin W, Cheng F (2020) Network-based drug repurposing for novel coronavirus 2019-nCoV/SARS-CoV-2. Cell Discov 6(1):14. https://doi.org/10.1038/s41421-020-0153-3

14. Shionoya et al (2021) Mefloquine, a potent anti-severe acute respiratory syndrome-related coronavirus 2 (SARS-CoV-2) drug as an entry inhibitor in vitro. Front Microbiol 12. 2021, [Online]. Available: https://www.frontiersin.org/article/https://doi.org/10.3389/fmicb.2021.651403

15. Fuzimoto AD (2021) An overview of the anti-SARS-CoV-2 properties of Artemisia annua, its antiviral action, protein-associated mechanisms, and repurposing for COVID-19 treatment. J Integr Med 19(5):375–388. https://doi.org/10.1016/j.joim.2021.07.003

16. Colson P, Rolain J-M, Lagier J-C, Brouqui P, Raoult D (2020) Chloroquine and hydroxychloroquine as available weapons to fight COVID-19. Int J Antimicrob Agents 55(4):105932. https://doi.org/10.1016/j.ijantimicag.2020.105932

17. Jain MK et al (2021) 525 Atovaquone for treatment of COVID-19 (Ataq COVID-19) trial. Open Forum Infect Dis 8(Supplement_1):S363–S364. https://doi.org/10.1093/ofid/ofab466.724

18. Jain MK et al (2022) Atovaquone for treatment of COVID-19: a prospective randomized, double-blind, placebo-controlled clinical trial. Front Pharmacol 13. https://doi.org/10.3389/fphar.2022.1020123

19. Puhl AC et al (2022) Pyronaridine protects against SARS-CoV-2 infection in mouse. ACS Infect Dis 8(6):1147–1160. https://doi.org/10.1021/acsinfecdis.2c00091

20. EBioMedicine (2021) COVID-19 and malaria, a tale of two diseases. EBioMedicine 70:103554. https://doi.org/10.1016/j.ebiom.2021.103554

21. Sachdeva C, Wadhwa A, Kumari A, Hussain F, Jha P, Kaushik NK (2020) In silico potential of approved antimalarial drugs for repurposing against COVID-19. Omi A J Integr Biol 24(10):568–580. https://doi.org/10.1089/omi.2020.0071

22. Cao R et al (2020) Anti-SARS-CoV-2 potential of artemisinins in vitro. ACS Infect Dis 6(9):2524–2531. https://doi.org/10.1021/acsinfecdis.0c00522

23. Hu Y et al (2021) Artemether, artesunate, arteannuin B, echinatin, licochalcone B and andrographolide effectively inhibit SARS-CoV-2 and related viruses in vitro. Front Cell Infect Microbiol 11. https://doi.org/10.3389/fcimb.2021.680127.

24. Gendrot M et al (2020) Antimalarial drugs inhibit the replication of SARS-CoV-2: an in vitro evaluation. Travel Med Infect Dis 37:101873. https://doi.org/10.1016/j.tmaid.2020.101873

25. Ianevski A et al (2020) Potential antiviral options against SARS-CoV-2 infection. Viruses 12(6):642. https://doi.org/10.3390/v12060642

26. Große M et al (2021) Quinine inhibits infection of human cell lines with SARS-CoV-2. Viruses 13(4):647. https://doi.org/10.3390/v13040647

27. (2020) Dexamethasone in hospitalized patients with COVID-19. N Engl J Med 384(8):693–704. https://doi.org/10.1056/NEJMoa2021436

28. Noreen S, Maqbool I, Madni A (2021) Dexamethasone: therapeutic potential, risks, and future projection during COVID-19 pandemic. Eur J Pharmacol 894:173854. https://doi.org/10.1016/j.ejphar.2021.173854

29. Cheng F-J et al (2021) "Hesperidin is a potential inhibitor against SARS-CoV-2 infection. Nutrients 13:8. https://doi.org/10.3390/nu13082800

30. NCT04452799, "Hesperidin and diosmin for treatment of COVID-19," https://clinicaltrials.gov/show/NCT04452799, 2020, [Online]. Available:https://www.cochranelibrary.com/central/doi/10.1002/central/CN-02134028/full

31. Montealegre-Gómez G, Garavito E, Gómez-López A, Rojas-Villarraga A, Parra-Medina R (2021) Colchicine: a potential therapeutic tool against COVID-19. Experience of 5 patients. Reumatol Clínica 17(7):371–375. https://doi.org/10.1016/j.reuma.2020.05.001

32. Lo HS et al (2021) Simeprevir potently suppresses SARS-CoV-2 replication and synergizes with remdesivir. ACS Cent Sci 7(5):792–802. https://doi.org/10.1021/acscentsci.0c01186

33. Muturi E et al (2022) Effects of simeprevir on the replication of SARS-CoV-2 in vitro and in transgenic hACE2 mice. Int J Antimicrob Agents 59(1):106499. https://doi.org/10.1016/j.ijantimicag.2021.106499

34. Salari S, Karbasforooshan H, Hosseinjani H (2022) Anti-HIV integrase inhibitors as new candidates for the treatment of COVID-19: a narrative literature review. Anti-Infec Agents 20(2). https://doi.org/10.2174/2211352519666210928110627

35. Stoeckle K et al (2020) COVID-19 in hospitalized adults with HIV .Open Forum Infect Dis 7(8). https://doi.org/10.1093/ofid/ofaa327

36. Waters L, Marra F, Pozniak A, Cockburn J, Boffito M (2022) Ritonavir and COVID-19: pragmatic guidance is important. Lancet 399(10334):1464–1465. https://doi.org/10.1016/S0140-6736(22)00280-X

37. Pereira M, Vale N (2022) Saquinavir: from HIV to COVID-19 and cancer treatment. Biomolecules 12(7):944. https://doi.org/10.3390/biom12070944

38. Bello M, Martínez-Muñoz A, Balbuena-Rebolledo I (2020) Identification of saquinavir as a potent inhibitor of dimeric SARS-CoV2 main protease through MM/GBSA. J Mol Model 26(12):340. https://doi.org/10.1007/s00894-020-04600-4

39. Horby PW et al (2020) Lopinavir–ritonavir in patients admitted to hospital with COVID-19 (RECOVERY): a randomised, controlled, open-label, platform trial. Lancet 396(10259):1345–1352. https://doi.org/10.1016/S0140-6736(20)32013-4

40. Indu P, Rameshkumar MR, Arunagirinathan N, Al-Dhabi NA, ValanArasu M, Ignacimuthu S (2020) Raltegravir, indinavir, tipranavir, dolutegravir, and etravirine against main protease and RNA-dependent RNA polymerase of SARS-CoV-2: a molecular docking and drug repurposing approach. J. Infect. Public Health 13(12):1856–1861. https://doi.org/10.1016/j.jiph.2020.10.015

41. Risner KH et al (2020) Maraviroc inhibits SARS-CoV-2 multiplication and s-protein mediated cell fusion in cell culture. BioRxiv the preprint server for biology. https://doi.org/10.1101/2020.08.12.246389

42. Shamsi A et al (2020) Glecaprevir and Maraviroc are high-affinity inhibitors of SARS-CoV-2 main protease: possible implication in COVID-19 therapy. Biosci Rep. 40(6):BSR20201256. https://doi.org/10.1042/BSR20201256

43. Roozbeh F et al (2021) Sofosbuvir and daclatasvir for the treatment of COVID-19 outpatients: a double-blind, randomized controlled trial. J Antimicrob Chemother 76(3):753–757. https://doi.org/10.1093/jac/dkaa501

44. Abbass S et al (2021) Efficacy and safety of sofosbuvir plus daclatasvir or ravidasvir in patients with COVID-19: a randomized controlled trial. J Med Virol 93(12):6750–6759. https://doi.org/10.1002/jmv.27264

45. Ohashi H et al (2021) Potential anti-COVID-19 agents, cepharanthine and nelfinavir, and their usage for combination treatment. iScience 24(4):102367. https://doi.org/10.1016/j.isci.2021.102367

46. Halder UC (2021) Predicted antiviral drugs darunavir, amprenavir, rimantadine and saquinavir can potentially bind to neutralize SARS-CoV-2 conserved proteins. J Biol Res (Thessalonike, Greece) 28(1):18. https://doi.org/10.1186/s40709-021-00149-2

47. Di Castelnuovo A et al (2021) "Lopinavir/ritonavir and darunavir/cobicistat in hospitalized COVID-19 patients: findings from the multicenter Italian CORIST study ," *Frontiers in Medicine*, vol. 8. 2021, [Online]. Available: https://www.frontiersin.org/articles/https://doi.org/10.3389/fmed.2021.639970

48. Harrison C (2020) "Coronavirus puts drug repurposing on the fast track.," *Nature biotechnology*, vol. 38, no. 4. United States, pp. 379–381, https://doi.org/10.1038/d41587-020-00003-1.

49. Gimeno A et al (2020) Prediction of novel inhibitors of the main protease (M-pro) of SARS-CoV-2 through consensus docking and drug reposition. Int J Mol Sci 21(11):3793. https://doi.org/10.3390/ijms21113793

50. Scroggs SLP et al (2020) Old drugs with new tricks: efficacy of fluoroquinolones to suppress replication of flaviviruses. Viruses 12(9):1022. https://doi.org/10.3390/v12091022

51. Taguchi Y, Turki T (2020) A new advanced in silico drug discovery method for novel coronavirus (SARS-CoV-2) with tensor decomposition-based unsupervised feature extraction. PLoS One 15(9):e0238907. https://doi.org/10.1371/journal.pone.0238907

52. Hu Y, Wei X, Zhu Q, Li L, Liao C, Jiang G (2022) COVID-19 pandemic impacts on humans taking antibiotics in China. Environ Sci Technol 56(12):8338–8349. https://doi.org/10.1021/acs.est.1c07655

53. Mustafa L, Tolaj I, Baftiu N, Fejza H (2021) Use of antibiotics in COVID-19 ICU patients. J Infect Dev Ctries 15(04):501–505. https://doi.org/10.3855/jidc.14404

54. Yacouba A, Olowo-okere A, Yunusa I (2021) Repurposing of antibiotics for clinical management of COVID-19: a narrative review.

Ann Clin Microbiol Antimicrob 20(1):37. https://doi.org/10.1186/s12941-021-00444-9

55. Goldstein EJC, Tillotson G, Redell M (2020) Antimicrobial management of respiratory infections in severe acute respiratory syndrome coronavirus 2 patients: clinical and antimicrobial stewardship programs conundrums. Open Forum Infect Dis 7(11):ofaa517. https://doi.org/10.1093/ofid/ofaa517

56. Damanhouri ZA, Alkreathy HM, Ali AS, Karim S (2021) The potential role of fluoroquinolones in the management of COVID-19 a rapid review. J Adv Pharm Educ Res 11(1):128–134. https://doi.org/10.51847/fe1ioiptwd

57. Scroggs SLP et al (2020) Fluoroquinolone antibiotics exhibit low antiviral activity against SARS-CoV-2 and MERS-CoV. Viruses 13(1):8. https://doi.org/10.3390/v13010008

58. Karampela I, Dalamaga M (2020) Could respiratory fluoroquinolones, levofloxacin and moxifloxacin, prove to be beneficial as an adjunct treatment in COVID-19? Arch Med Res 51(7):741–742. https://doi.org/10.1016/j.arcmed.2020.06.004

59. Marciniec K, Beberok A, Pęcak P, Boryczka S, Wrześniok D (2020) Ciprofloxacin and moxifloxacin could interact with SARS-CoV-2 protease: preliminary in silico analysis. Pharmacol Reports 72(6):1553–1561. https://doi.org/10.1007/s43440-020-00169-0

60. Gordon JC, Myers JB, Folta T, Shoja V, Heath LS, Onufriev A (2005) H++: a server for estimating p Ka s and adding missing hydrogens to macromolecules. Nucleic Acids Res. 33(suppl_2):W368–W371. https://doi.org/10.1093/nar/gki464

61. Anandakrishnan R, Aguilar B, Onufriev AV (2012) "H++ 3.0: automating pK prediction and the preparation of biomolecular structures for atomistic molecular modeling and simulations. Nucleic Acids Res 40, no. Web Server issue, pp. W537–41. https://doi.org/10.1093/nar/gks375

62. Trott O, Olson AJ (2010) AutoDock Vina: improving the speed and accuracy of docking with a new scoring function, efficient optimization, and multithreading. J Comput Chem 31(2):455–461. https://doi.org/10.1002/jcc.21334

63. Morris GM, Huey R, Olson AJ (2008) Using AutoDock for ligand-receptor docking. Curr Protoc Bioinforma 24(1). https://doi.org/10.1002/0471250953.bi0814s24

64. Biovia DS (2016) BIOVIA discovery studio visualizer. Softw version 20:779

65. Jo S, Kim T, Iyer VG, Im W (2008) CHARMM-GUI: a web-based graphical user interface for CHARMM. J Comput Chem 29(11):1859–1865. https://doi.org/10.1002/jcc.20945

66. Brooks BR et al (2009) CHARMM: the biomolecular simulation program. J Comput Chem 30(10):1545–1614. https://doi.org/10.1002/jcc.21287

67. Lee J et al (2016) Charmm-Gui Input Generator For Namd, Gromacs, Amber, Openmm, And Charmm/Openmm Simulations Using The Charmm36 Additive Force Field. J Chem Theory Comput 12(1):405–413. https://doi.org/10.1021/acs.jctc.5b00935

68. Best RB et al (2012) Optimization of the additive CHARMM all-atom protein force field targeting improved sampling of the backbone ϕ, ψ and side-chain χ1 and χ2 dihedral angles. J Chem Theory Comput 8(9):3257–3273. https://doi.org/10.1021/ct300400x

69. Phillips JC et al (2005) Scalable molecular dynamics with NAMD. J Comput Chem 26(16):1781–1802. https://doi.org/10.1002/jcc.20289

70. Jorgensen WL, Chandrasekhar J, Madura JD, Impey RW, Klein ML (1983) Comparison of simple potential functions for simulating liquid water. J Chem Phys 79(2):926–935. https://doi.org/10.1063/1.445869

71. Yu W, He X, Vanommeslaeghe K, MacKerell AD Jr (2012) Extension of the CHARMM general force field to sulfonyl-containing compounds and its utility in biomolecular simulations. J Comput Chem 33(31):2451–2468. https://doi.org/10.1002/jcc.23067

72. Nosé S, Klein ML (1983) Constant pressure molecular dynamics for molecular systems. Mol Phys 50(5):1055–1076. https://doi.org/10.1080/00268978300102851

73. Grest GS, Kremer K (1986) Molecular dynamics simulation for polymers in the presence of a heat bath. Phys Rev A, Gen Phys 33(5):3628–3631. https://doi.org/10.1103/physreva.33.3628

74. Darden T, York D, Pedersen L (1993) Particle mesh Ewald: an N·log(N) method for Ewald sums in large systems. J Chem Phys 98(12):10089–10092. https://doi.org/10.1063/1.464397

75. Essmann U, Perera L, Berkowitz ML, Darden T, Lee H, Pedersen LG (1995) A smooth particle mesh Ewald method. J Chem Phys 103(19):8577–8593. https://doi.org/10.1063/1.470117

76. Kumar S, Thambiraja TS, Karuppanan K, Subramaniam G (2022) Omicron and Delta variant of SARS-CoV-2: a comparative computational study of spike protein. J Med Virol 94(4):1641–1649. https://doi.org/10.1002/jmv.27526

77. Reva BA, Finkelstein AV, Skolnick J (1998) What is the probability of a chance prediction of a protein structure with an rmsd of 6 å? Fold Des 3(2):141–147. https://doi.org/10.1016/S1359-0278(98)00019-4

78. Lobanov MY, Bogatyreva NS, Galzitskaya OV (2008) Radius of gyration as an indicator of protein structure compactness. Mol Biol 42(4):623–628. https://doi.org/10.1134/S0026893308040195

79. Bogatyreva NS, Ivankov DN (2008) The relationship between the solvent-accessible surface area of a protein and the number of native contacts in its structure. Mol Biol 42(6):932. https://doi.org/10.1134/S0026893308060150

80. Shaytan AK, Shaitan KV, Khokhlov AR (2009) Solvent accessible surface area of amino acid residues in globular proteins: correlation of apparent transfer free energies with experimental hydrophobicity scales. Biomacromol 10(5):1224–1237. https://doi.org/10.1021/bm8015169

Authors and Affiliations

Eslam A. R. Mohamed[1] · **Islam M. Abdel-Rahman[2]** · **Magdi E. A. Zaki[3]** · **Ahmad Al-Khdhairawi[4]** ·
Mahmoud M. Abdelhamid[5] · **Ahmad M. Alqaisi[6,7]** · **Lyana binti Abd Rahim[8]** · **Bilal Abu-Hussein[9,10]** ·
Azza A. K. El-Sheikh[11] · **Sayed F. Abdelwahab[12]** · **Heba Ali Hassan[13]**

Eslam A. R. Mohamed
eslamahmedragabmohamed@gmail.com

Islam M. Abdel-Rahman
dr.islam_moh@deraya.edu.eg

Magdi E. A. Zaki
mezaki@imamu.edu.sa

Ahmad Al-Khdhairawi
ahmadayad@outlook.my

Mahmoud M. Abdelhamid
mahmod.albakry@gmail.com

Ahmad M. Alqaisi
ahmadayad@outlook.my

Lyana binti Abd Rahim
lyanaabd.rahim@yahoo.com

Bilal Abu-Hussein
asad.bilaldr@gmail.com

Azza A. K. El-Sheikh
aaelsheikh@pnu.edu.sa

Sayed F. Abdelwahab
s.fekry@tu.edu.sa

1   Department of Chemistry, Faculty of Science, Minia University, Minia 61511, Egypt

2   Department of Pharmaceutical Chemistry, Faculty of Pharmacy, Deraya University, New-Minia 61519, Minia, Egypt

3   Department of Chemistry, Faculty of Science, Imam Mohammad Ibn Saud Islamic University (IMSIU), Riyadh, Saudi Arabia

4   Department of Biological Science and Biotechnology, Faculty of Science and Technology, Universiti Kebangsaan Malaysia, 43600 Bangi, Selangor, Malaysia

5   Department of Pharmaceutical Chemistry, Faculty of Pharmacy, Al-Azhar University, Asyut 71524, Egypt

6   Chemistry Department, University of Jordan, Amman 11942, Jordan

7   Present Address: School for Engineering of Matter, Transport and Energy, Arizona State University, Tempe, AZ 85287, USA

8   Department of Medicine, Hospital Tuanku Ampuan Najihah, Kuala Pilah, Negeri Sembilan, Malaysia

9   Albayader Specialty Hospital, Amman, Jordan

10 Present Address: Department of General Surgery, Cumberland Infirmary Hospital, Carlisle, England

11 Basic Health Sciences Department, College of Medicine, Princess Nourah bint Abdulrahman University, P.O. 13 Box 84428, Riyadh 11671, Saudi Arabia

12 Department of Pharmaceutics and Industrial Pharmacy, College of Pharmacy, Taif University, PO Box 11099, Taif 21944, Saudi Arabia

13 Department of Pharmacognosy, Faculty of Pharmacy, Sohag University, Sohag 82524, Egypt